ACS OMEGA

http://pubs.acs.org/journal/acsodf

Article

About the Shape of the Crystallization Front of the Semiconductor Nanowires

Valery A. Nebol'sin, Elena V. Levchenko,* Vladimir Yuryev, and Nada Swaikat

Cite This: *ACS Omega* 2023, 8, 8263−8275

Read Online

ACCESS | Metrics & More | Article Recommendations

ABSTRACT: During the nanowire (NW) formation, the growth steps reaching the crystallization front (CF) under the catalytic drop are either absorbed by the three-phase line or accumulated in front of it, curving the surface of the front. In this paper, we have analyzed the conditions leading to a change of shape of the crystallization front of the NWs under the catalyst drop as well as the reasons for the formation of atomically smooth (singular) and curved (nonsingular) regions. A model explaining the curvature of the crystallization front under the drop in the process of NW growth is proposed. The model demonstrates that under conditions of good wettability of the crystalline surface with a catalytic liquid and nucleation at regular places of the growing NW face, a metastable equilibrium at the CF near the three-phase line is achieved due to the thermodynamic size effect of reduction of overcooling (supersaturation). This metastable equilibrium results in the curvature of the CF. The CF curvature depends on the NW radius and the level of overcooling (supersaturation) in the droplet. During this process, the low-index inclined facets adjacent to the wetting perimeter of the catalyst drop may appear on the curved CF.

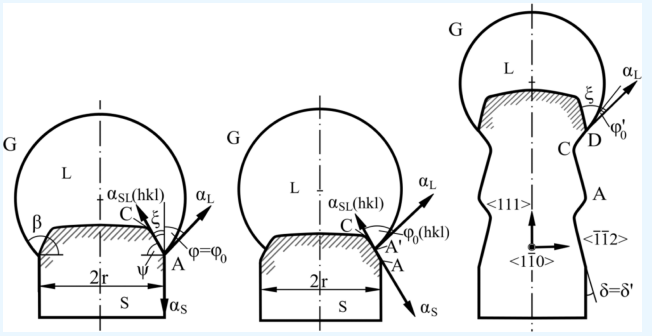

1. INTRODUCTION

Nanowires (NWs) are quasi-one-dimensional crystalline nanostructures with a very high length to diameter ratio. The specific shape, the microminiature dimensions, the highest structural perfection, and the extraordinary ratio of the surface to the volume of such crystals give NWs a number of unique and advanced physical properties. In addition, the NWs of the semiconductors (Si, Ge, GaAs, GaP, InAs, etc.) have some very interesting electronic, photon, and phonon properties.[1−5] Such unsurpassed characteristics of the NWs open a wide range of applications for them in the development of technology as well as in fundamental science.[3−7] In the last decade, the emergence of low-temperature methods for the catalytic synthesis of the NWs, according to the vapor−liquid−solid (VLS) scheme and high-resolution tools for studying their crystal structure, made it possible to move to a systematic research of NWs and provided breakthroughs in (i) in situ growth control with an atomic resolution; (ii) the development of phase engineering methods; and (iii) the creation of NW heterostructures and quantum dots or disks, opening up new horizons in the field of crystal growth.[8−13]

However, despite the breathtaking direct methods of observing the atomic stacking of layers during the NW growth, the understanding of the physics behind the complex growth mechanisms and phenomena accompanying VLS growth still lags behind the experimental achievements. For example, there is still a lack of a comprehensive thermodynamic explanation of the morphological instability of the crystallization front (CF) during the NW growth process. It was previously supposed that the CF under the catalyst drop can only be flat. Only recently, in situ transmission electron microscopy (TEM) breakthrough studies have found that the CF in Si, Ge, GaP, −Alα_2O_3, and GaAs NWs have grown with liquid-phase particles of Au, Ga, Cu, and Al metals (Me), as well as discovering that the Au−Ga and Au−Al alloys can be curved near the three-phase boundary and is convex toward the liquid phase.[4−6,8,9] Therefore, according to the important in situ observations by Wen et al.,[9] Gamalski et al.,[10] Oh et al.,[11] and Jacobsson et al.,[14] a truncated face is present on the periphery of a NW CF. This truncated face determines the location of the crystal nucleus inside the droplet and leads to a crystalline phase of the zinc-blende (ZB) type.[15,16]

A deviation of CF from a flat shape can lead to many effects, such as changes in the spatial direction of the NW growth, an uneven distribution of the dopant impurity in the volume of the crystal, the appearance of inclusions, the formation of

Received: October 7, 2022
Accepted: February 8, 2023
Published: February 23, 2023

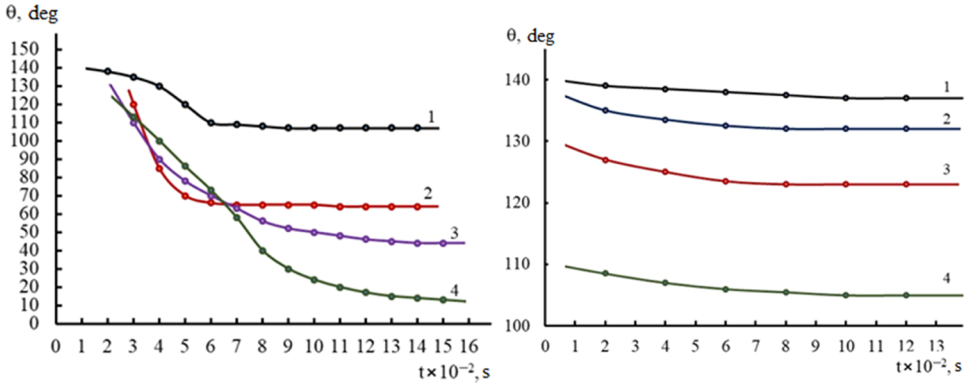

Figure 1. Time dependencies of the contact angle θ during wetting of {111} Si substrates by Sn (line 1), Cu (line 2), Ag (line 3), and Au (line 4) drops (a) and alloys Sn + 5.0 atom % Si (line 1), Zn + 15.0 atom % Si (line 2), Cu + 36.1 atom % Si (line 3), and Au + 38.4 atom % Si (line 4) (b) at 1473 K in the stream of H_2.

lateral cutting, twinning, the conversion of the crystal structure, etc.[15,17] The formation of structurally sharp heterojunctions and the occurrence of spontaneous polytypism in the NW of $A^{III}B^{V}$ compounds also largely depend on the shape of the CF.[15,17,18] With the morphological instability of CF, capillary instability of the meniscus of the Me catalyst drop can also be observed, leading to the distortion of the cross-section of the NW and bends and branching of crystals.[19] In this work, we aim (i) to analyze the conditions leading to a change in the shape of CF during the NW growth and (ii) to provide thermodynamic reasoning for the formation of singular and nonsingular regions on the CF.

In this paper, we reveal the physical nature of the mechanism of curvature of the flat CF under a drop of the catalyst near the tree-phase line (TL). We show that with the NW diameter decreasing, a complete phase equilibrium at the front can be achieved by a combination of temperature T and the radius of curvature r_c. We also suppose that the appearance of an inclined (oblique) facet adjacent to the TL on a curved CF is possible as a result of the presence of singular minima on the angular (orientational) dependence of the specific free surface energy (SFSE).

Our results are of great fundamental importance for the physics of crystallization and provide a clear way to control the growth processes of IV, III–V, and II–VI semiconductor NWs.

2. EXPERIMENTAL PROCEDURE

Si, Ge, and Si_xGe_{1-x} NWs were grown using a[17,19] technique on Si(111) substrates by a molecular beam epitaxy (MBE) method and a chemical vapor deposition (CVD) method, which were at temperatures of 773–1373 K with Au, Ni, Pt, Pd, Ag, and Cu particles as catalysts for the growth process. The diameter of the particles ranged from 30 nm to 20 μm. The following chemical systems were used: $SiCl_4 + H_2$ and $GeCl_4 + H_2$. Hydrogen (H_2) was used for growing a silicon NW, which had a dew point of 215 K and contained 10^{-3}% O_2; so, it was subjected to additional purification and drying in a gas purification plant. The results of refs 9–11 and 20 were also used for analysis. In ref 18, GaAs NWs were grown by MBE on Si(111) substrates at temperatures of 600–800 K using Au catalytic particles with an average diameter of 20 nm. In refs 8 and 9, Si, Ge, and GaP NWs were grown in an ultra-high-vacuum transmission electron microscope (TEM) and also on prepurified Si(111) substrates. For the catalysts of the VLS process, we used particles of Au and Cu as well as Au–Ga and Au–Al alloys obtained by the thermal spraying of 0.1–1 nm thick films in the vacuum and their subsequent separation into droplets during annealing. Then, the particles of metals and alloys were exposed to gases: either disilane or digermane. To investigate the growth of GaP NWs, Si substrates with particles of Au–Ga and Au–Al alloys were heated when they were exposed to triethyl gallium in an excess amount of phosphine. The Si NWs were grown with the participation of Au particles at a temperature of 823 K and a partial pressure of Si_2H_6 5.33×10^{-5} Pa, as well as with the participation of Cu at a temperature of 803 K and a partial pressure of Si_2H_6 2.66×10^{-5} Pa.[8] The Ge NWs were obtained with an Au catalyst at 683 K and a pressure of Ge_2H_6 5.33×10^{-4} Pa, and the GaP NWs were synthesized with particles of Au–Ga or Au–Al alloys at T = 723 K and a pressure of 1.33×10^{-3} alloy Pa.[8,9]

The grown NWs were studied by scanning (SEM) and transmission electron microscopy (TEM). In special cases, the thin sections of the NWs were manufactured for metallographic studies. The morphology time evolution of the CF in the vicinity of the three-phase line (TL) was studied in situ by TEM methods using video images obtained at a speed of 30 frames/s.[8,9] To find the values of the contact angle on the TEM and SEM images of the droplets during the wettability study of {111} Si substrates, any two of the three values characterizing the droplet on the substrate were measured: the radius of curvature of the surface of the droplet R, the diameter of its base d ($d = 2r$), and the height H. The contact angle was calculated as

$$\theta = 2\,\mathrm{arctg}\frac{2H}{d} = \arccos\left(1 - \frac{H}{R}\right) = \begin{cases} \arcsin\dfrac{d}{2R}, & \theta < 90^\circ \\ 180^\circ - \arcsin\dfrac{d}{2R}, & \theta > 90^\circ \end{cases} \quad (1)$$

where θ is the contact angle of the catalytic drop on the substrate.

https://doi.org/10.1021/acsomega.2c06475
ACS Omega 2023, 8, 8263–8275

3. RESULTS AND DISCUSSION

3.1. Experimental Results. Experiments and analysis of the literature show that NWs of Si, Ge, GaAs, GaP, Si_xGe_{1-x}, and other semiconductor materials in contact with saturated solutions of liquid droplets of the Me catalyst usually have smooth solid/liquid interfaces. These interfaces are frequently represented by one transverse close-packed face of {111} type.[15,17,19,21,22] In the process of stationary growth of NWs, the CF remains stable, and the crystals rapidly develop in one crystallographic direction. For example, Si and Ge NWs, which have the structure of a diamond cubic lattice, usually have the ⟨111⟩ growth axis orientation and the {111} end face.[17,19] The results of the wettability study of {111} Si substrates by the droplets of metal catalysts for the NW growth are shown in Figure 1.

Figure 1 shows that metals such as Sn do not wet a solid silicon ($\theta > 90°$), while Au and Ag wet solid silicon well ($\theta \ll 90°$). For droplets saturated with crystallizable substance, Me−Si, we got angle $\theta > 90°$. A flat NW front (Figure 2) is formed when the crystal surface is poorly wetted by a catalyst drop, for example, in Cu−Si, Cu−Si_xGe_{1-x}, etc. systems at T = 1273 K.[19]

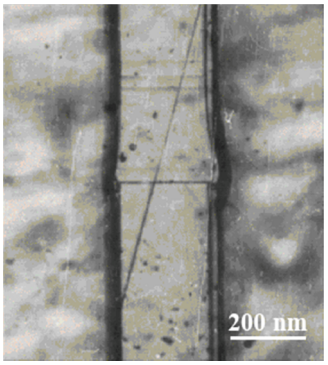

Figure 2. Etched cross-section of Si⟨111⟩ NW doped with boron in the process of growth through droplets Cu−Si at T = 1273 K. The image clearly shows a flat crystallization front, represented by a transverse close-packed face of the {111} family.

At the initial stage of growth from the substrate, the CF is concave (Figure 3a) but then gradually becomes flat (Figure 3b,c).

At good wettability by the catalyst drop, the surface of the CF crystal is curved (Figure 4). In the TL region, the CF is strongly curved toward the liquid phase. The radius of curvature of the CF near the TL is approximately 2−10% of the radius of the NW.

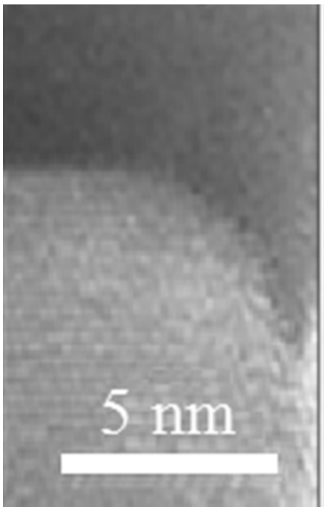

Figure 4. SEM image of the curved section of a nanowire crystallization front near the three-phase line in the Ag−Si system.

We also found that on the lateral surface of the NW, the formation of facets is possible due to the release of oblique close-packed faces that occur at the crystallization front near the TL. Facets are a sequence of alternating flat microgrids inclined at an angle of ∼20° to the growth axis and rough areas of the isotropic surface of the NW (Figure 5).

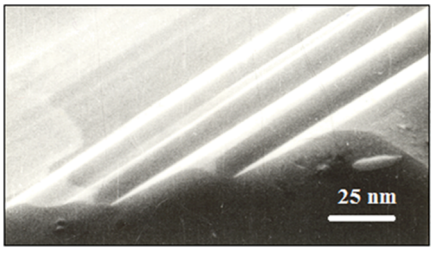

Figure 5. Morphology of the lateral surface of silicon NW, consisting of sickle-shaped alternating regions. Each section is a step cut by a plane of {111} and has a curved isotropic end.

Let us first consider the conditions for the formation of a flat CF.

3.2. Formation of the Flat Crystallization Front. Since the saturated vapor pressure of the crystallizable NW matter is

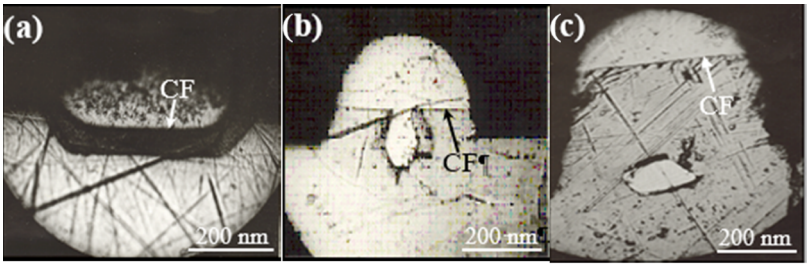

(a) ×2000 (b) ×1875 (c) ×1875

Figure 3. Thin sections of the Si NWs illustrate that at the initial growth stage, the CF is concave (a) and then becomes flat (b, c). The capture of a two-component alloy by a moving front during rapid NW crystallization is shown in (b) and (c) photos.

https://doi.org/10.1021/acsomega.2c06475
ACS Omega 2023, 8, 8263−8275

significantly less than the similar vapor pressure of the Me catalyst and the crystallizable matter is solid at the growth temperature, then, in this case, we have the dissolution of the solid matter in the melt of the liquid metal (see Figure 2). Let us assume that (i) the substance that forms a NW is a pure substance, i.e., a substance whose molecules are all the same, and (ii) a mixture of atoms of a crystalline substance with a liquid Me catalyst is a solution. The semiconductor NWs in contact with saturated solutions of catalyst droplets, in contrast to their own melt, have a smooth solid/liquid interface because, in solutions, their atoms are much more diluted. For example, the ratio of the content of Si (% (atomic)) to the metal content (% (atomic)) in a solution of Me−Si at T = 1373 K is 0.25 for Zn−Si; 0.57 for Ag−Si; 1.12 for Al−Si; 1.50 for Au−Si; and 2.33 for Pt−Si.[23]

An atom of Si and Ge (or the atomic complex Ga−As, Ga−P, etc.), appearing at the end face of the NW during crystallization from a solution of a catalyst drop, can be adsorbed on it and lose some of its dissolution heat (melting heat) q, and then start moving along this surface until one of the following events occurs: (i) either the atom acquires enough energy to go back into the liquid solution of the drop, (ii) it will be in one position or another on the step where the number of neighbors is enough to hold the atom here, (iii) it will reach the edge of the face and be absorbed by the TL adjacent to the face, (iv) on the contrary, such atoms will accumulate in front of it in the form of growth steps, or (v) it will meet a number of other mobile adsorbed atoms, which is sufficient for the formation of a stable nucleus of a new layer.[15,17,22] The latter case is possible only when the concentration of atoms on the surface is high and the contact angles β of the droplet are large.[23] But it is most likely that a NW grows by the lateral propagation of the edge steps and the addition of atoms to the nucleus appearing at the three-phase boundary (TL nucleation[24,25]). In both cases, the surface of the CF tends to remain smooth, and its irregularities must be smoothed out because each step grows to its possible limits. It will either meet another step and merge with it or, after reaching the surface of the edge of the face, will be absorbed by the TL and cease to exist as a step.[8,19] Such growth occurs, for example, when a GaAs NW with a WZ structure in the Ga−GaAs system has contact angles of 100−125° for the Ga droplet at the top of the NW.[8,15]

If the CF under the droplet is flat, then it is due to the presence of singular orientations, for which the SFSE of crystal α_S has a sharp minimum α_S = min, and the angular derivative $\frac{\partial \alpha_S}{\partial \psi}$ has a sufficiently large value[24] (Figure 6), where ψ is the angle of deviation of the crystal surface from the singular face, for example, {111} or {0001}. Such minimization of the SFSE leads to the fact that in the steady state, the NW radius, the radius of the catalyst drop, and the TL remain constant during the growth.

Thus, if the volume of the droplet does not change during the growth, then the radius of the TL coincides with the NW radius, and the angle of inclination of the lateral surface of the crystal to the horizontal (transverse singular face) is δ, which is equal to 90° (δ = 90°). Nucleation on the flat transverse face of the CF {111} requires noticeable overcooling (supersaturation) in the droplet, and layer-by-layer growth takes place. In this case, the TL serves as the source of the layers, and the steps are easily formed and/or absorbed by the TL.[8,15,19,23]

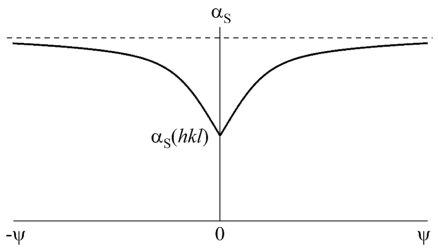

Figure 6. Angular (orientational) dependence of the SFSE α_S, illustrating the anisotropy of the crystal SFSE in the vicinity of the singular face with small crystallographic indices {hkl}.[24,26] Reprinted with permission from Burton, W. K.; Cabrera, N.; Frank, F. C. The Growth of Crystals and the Equilibrium of Their Surfaces. Philos. Trans. R. Soc., A **1951**, *243*, 299−358. Copyright 1951 The Royal Society (U.K.).

The actual size of the critical nucleus for any given degree of overcooling can be calculated if the value of the SFSE of a solid/liquid boundary α_{SL} is known.

Consider a system where a liquid and a solid are at constant pressure and temperature. The change in the free energy of the system is the result of a phase transformation associated with the bulk component of the transition of matter from the liquid phase to the solid phase, which can be written as $dG_P = dH - T\,dS$ for a constant number of moles of all of the components or, integrating, $\Delta G_P = \Delta H - T\Delta S$. At the equilibrium temperature of the phase transition (in our case, crystallization) for bulk samples T_E, the value of change of free energy ΔG_P is zero, $\Delta G_P = 0$.

It follows that the change in entropy during the phase transition $\Delta S = \Delta H/T_E = (S_L - S_S)$, where ΔH is the latent molar heat of the release of the crystallizable substance from the solution, equal to the energy difference between the liquid H_L and solid H_S phases (can be denoted as L_m). Now we can write

$$\Delta G_P = \Delta H - \frac{T\Delta H}{T_E} = \frac{\Delta H(T_E - T)}{T_E} = \frac{L_m \Delta T}{T_E} \quad (2)$$

where $\Delta T = T_E - T$ is the overcooling of the liquid phase near the solid/liquid boundary, and T is the actual temperature of the crystallization process. Here, the equilibrium temperature T_E is a temperature at which the free energy values of the phases separated by a flat surface and under the same pressure are equal.

The chemical potential for each component in the solution can be written as $\mu = \left(\frac{dG}{dN_i}\right)_{p,T,N_j}$, where N_i is the number of particles of component i in the system. Here, N_j means the constancy of all N, except N_j. Going from thermodynamic potential change to the chemical potential change of the crystallizable matter, eq 2 for the undistorted liquid-phase catalyst $\overline{\mu}_L$ and a flat crystal $\overline{\mu}_S$ can be written as

$$\Delta\overline{\mu}_{LS} = q\frac{\Delta T}{T_E} \quad (3)$$

where q is the latent heat release of the crystallizable matter from the solution, calculated per atom.

Since the surface of the catalytic liquid is curved during the NW growth,[27] we can write the expression for the isobaric isothermal Gibbs potential of the crystallizable substance in the

https://doi.org/10.1021/acsomega.2c06475
ACS Omega 2023, 8, 8263−8275

liquid drop of the catalyst in the form of eq 4. By taking into account mass transfer, we get

$$dG = -S\,dT + V\,dp + \mu_L\,dn \tag{4}$$

where n is the number of moles of the substance, and the chemical potential of a substance in the liquid phase can be expressed as $\mu_L = \left(\frac{\partial G}{\partial n}\right)_{T,p}$ and volume as $V = \left(\frac{\partial G}{\partial p}\right)_{T,n}$.

For an individual substance, $V = V_m$ (molar volume). Then, at T = const, we have

$$\left(\frac{\partial \mu}{\partial p}\right)_T = \left[\frac{\partial}{\partial p}\left(\frac{\partial G}{\partial n}\right)\right]_T \left[\frac{\partial}{\partial n}\left(\frac{\partial G}{\partial p}\right)\right]_T = \left(\frac{\partial V}{\partial n}\right)_T = V_m \tag{5}$$

From here, at T = const, we get $\mu_L = V_m\,dp$. If the change in pressure occurs only due to the curvature change, then from eq 5, we obtain

$$d\tilde{\mu}_L = V_m\,dp = V_m\,d\left(\frac{2\alpha_L}{R}\right) \tag{6}$$

where $d\tilde{\mu}_L$ is the change in the chemical potential of the crystallizable substance in the liquid phase due to a change in its curvature, α_L is the SFSE of the liquid/vapor phase interface, and R is the radius of curvature of the catalyst droplet at the NW top.

The integration of eq 6 with limits of integrations being from $R = \infty$ (for the flat surface of the macroscopic phase) to R (for the surface of the droplet) gives

$$\Delta\tilde{\mu}_L = \tilde{\mu}_L - \bar{\mu}_L = V_m\left(\frac{2\alpha_L}{R}\right) \tag{7}$$

According to eq 7, the chemical potential of the crystallizable substance in the macrophase is lower than in the microphase (nanodrop).

At the atomistic level, the chemical potential of the crystallizable substance in the curved liquid-phase droplet of a catalyst of a spherical shape of the radius R is

$$\tilde{\mu}_L = \bar{\mu}_L + \frac{2\alpha_L\Omega_L}{R} \tag{8}$$

where Ω_L is the volume occupied by one atom of the crystallizable substance in the liquid phase.

Considering the curvature of the droplet surface and the constant pressure, we can obtain the change in free energy ΔG. It corresponds to the formation under the droplet of the nucleus in the shape of a disk with the radius r_N and a monoatomic height h on the flat surface of the CF. This change in free energy consists of two summands: the "volumetric" term (a negative sign is for temperatures T below T_E) and the "surface" (second) term

$$\Delta G = -\frac{\pi r_N^2 h}{\Omega_S}\left(q\frac{\Delta T}{T_E} + \frac{2\alpha_L\Omega_L}{R}\right) + 2\pi r_N h\alpha_{SL} \tag{9}$$

where Ω_S is the specific volume of the atom in the solid phase and α_{SL} is the SFSE of the crystal/liquid phase interface (or solid/liquid interface). Here, $\left(q\frac{\Delta T}{T_E} + \frac{2\alpha_L\Omega_L}{R}\right) = \Delta\tilde{\mu}_{LS}$ is the effective difference in the chemical potentials of the crystallizable substance in the liquid and solid phases.

The change in ΔG in eq 9 is illustrated in Figure 7, which shows that the value of ΔG is positive for small r_N and negative

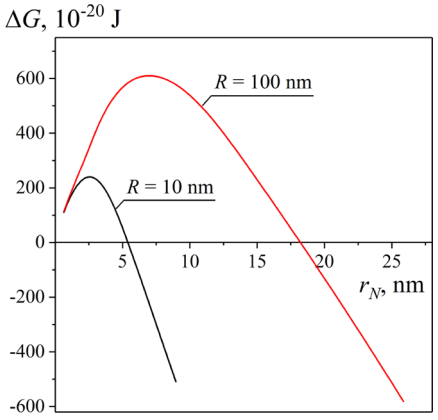

Figure 7. Change in free energy during crystallization from a small drop of a Me catalyst with a different R.

for large r_N values and depends on the radius R of the catalyst droplet, decreasing with a decrease of R. For a spherical drop, we assume that the radius of the curvature R and radius of the drop are equal.

The critical radius of the nuclear r_N^* under the drop of the catalyst is defined as a value for which the derivative of free energy ΔG with respect to r_N is zero. Therefore, at temperature $T_E - \Delta T$, the critical radius r_N^* can be found from $\left.\frac{d(\Delta G)}{dr_N}\right|_T = 0$, or

$$-\frac{2\pi r_N h}{\Omega_S}\left(q\frac{\Delta T}{T_E} + \frac{2\alpha_L\Omega_L}{R}\right) + 2\pi h\alpha_{SL} = 0 \tag{10}$$

which gives

$$r_N^* = \frac{\alpha_{SL}\Omega_S}{q\frac{\Delta T}{T_E} + \frac{2\alpha_L\Omega_L}{R}} \tag{11}$$

Figure 8 demonstrates the relationship between ΔT and r_N^* for two different radii of the catalyst droplet R. The upper branches (for positive values of ΔT and r_N^*) correspond to the growth of NWs from the supercooled liquid-phase catalyst, and the lower branches (for negative values of ΔT and r_N^*) relate to the formation of "negative" NWs from the liquid phase at a

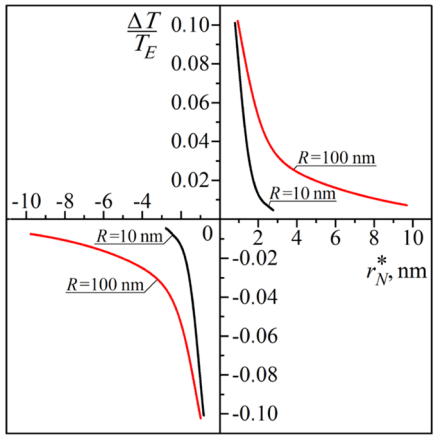

Figure 8. Relationship between the radius of the critical nucleus r_N^*, formed at regular surface sites under the catalyst drop, and overcooling of $\Delta T/T_E$.

https://doi.org/10.1021/acsomega.2c06475
ACS Omega 2023, 8, 8263−8275

temperature T above the temperature T_E, $\Delta T = T_E - T < 0$ (the negative curvature during overheating of the liquid).[28]

During the formation of the crystalline nucleus under the catalyst drop, the energy gain is related to the fact that the Gibbs energy of the new phase is significantly less than the energy of the original curved liquid phase, while the energy loss is attributable to the formation of the interface surface between the nucleus and the liquid phase (Figures 7 and 8). As the size of the nucleus increases, r_N, the energy passes through the maximum at the critical nucleus radius r_N^* (Figure 7). A further increase in the size of the nucleus leads to a decrease in the free energy ΔG (Figure 7). With a decrease in the radius of curvature of the drop of the catalyst R, i.e., during the transition to thinner NW, the critical nucleus radius r_N^* decreases at regular places of the surface under the drop. The radius of the catalyst drop R is uniquely related to the transverse size of the grown crystal r (NW radius) as $R = \frac{r}{\sin\beta}$. Therefore, in the case of nucleation at regular surface sites under the droplet, less overcooling (supersaturation) in the droplet is required for growing thinner NWs than for the thicker ones by the VLS mechanism. Here, $\beta = 90° + \varphi$ is the contact angle of the catalyst droplet at the top of the NW, and φ is the angle between the tangent to the liquid surface at point A on TL and the NW axis (see Figure 9).

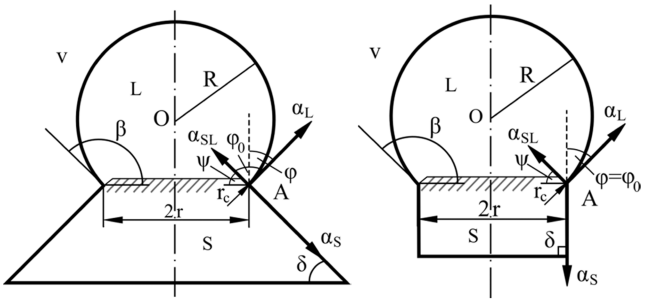

(a) (b)

Figure 9. Diagram of the three-phase interfaces, solid, liquid, and vaporous: (a) for the catalyst droplet at the top of the conical NW ($0 < \delta < 90°$) and (b) for cylindrical NW ($\delta = 90°$).

Indeed, in smaller droplets of the catalyst, the equilibrium solubility and supersaturation of growth particles can be achieved more easily compared to larger droplets (see eq 9 and Figure 7). The NW growth will occur only if the actual concentration of growth particles is higher than the equilibrium solubility. Therefore, it is possible to maintain the vapor pressure below the equilibrium concentration in large droplets by controlling the supersaturation in the vapor phase. In this case, the growth of the thickest NWs can be stopped. That is why technological processes, as a rule, implement the conditions for the NW growth at low temperatures (600−900 K) and supersaturations (0.01−0.02) in the vapor phase, and the growth rate of such crystals increases with a decrease of their diameter.[9,12,18]

When the flat face {111} of the CF is adjacent to the TL (Figure 9), the minimum increment of the free surface energy of the three-phase system during the nucleation and growth of the steps is achieved when[27]

$$\alpha_S \cos\delta = \alpha_{SL} + \alpha_L \cos\beta \quad (12)$$

where α_S is the SFSE of the crystal/vapor phase interface.

The angle of growth (crystallization),[27] i.e., the angle of equilibrium displacement of TL during NW growth $\varphi_0 = \beta - \delta$, can be determined using eq 12. If $\delta = 90°$, then from eq 12, we get the growth condition for NWs with a cylindrical lateral surface $\alpha_{SL} - \alpha_L \sin\varphi_0 = 0$.[17,19,22,24] If $\delta = 0°$, then eq 12 gives the condition of the mechanical equilibrium of the catalyst drop on a flat extended substrate $\alpha_S = \alpha_{SL} + \alpha_L \cos\theta$, where $\beta = \theta$, while θ is an equilibrium contact angle in the Young equation. The steps can be generated or absorbed by the three-phase separation line and form a lateral surface of the NW at an angle δ, if $(\beta - \delta) < \theta$. Therefore, the TL becomes a source of monoatomic steps at a significant difference of $(\theta - \varphi_0)$, i.e., at large values of θ (poor wettability) or small values of φ_0.

The growth rate of the steps generated by the TL is very high in comparison with the rate of their nucleation.[17] Therefore, the transverse NW surface {111} corresponds to almost flat CF under the drop with a small number of steps moving quickly from the TL (see Figure 1).[8]

The most frequently observed directions of growth of arsenide nanowires are direction $\langle\overline{1}11\rangle$ B for the zinc blende (ZB) structure or $(000\overline{1})$ for the wurtzite (WZ) type phase (Figure 10a,b), which also have a flat crystallization front.[15]

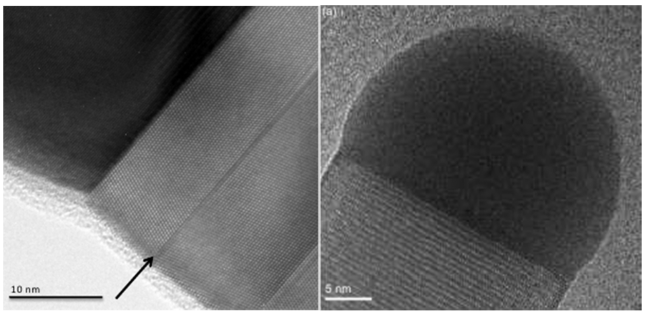

(a) (b)

Figure 10. GaAs NWs with a zinc blende structure in the top part of the crystal predominantly have a transverse close-packed $(\overline{1}11)$ B face (a), while those with a wurtzite structure have a $(000\overline{1})$ face (b). Reprinted with permission from Harmand, J.-C.; Patriarche, G.; Glas, F.; Panciera, F.; Florea, I.; Maurice, J.-L.; Travers, L.; Ollivier, Y. Atomic Step Flow on a Nanofacet. Phys. Rev. Lett. **2018**, *121* (16), 166101. Copyright 2018 American Physical Society. Reprinted from Dhalluin, F. Nanofils de Silicium: Dépôt chimique en phase vapeur assisté par catalyseurs métalliques et prémices d'intégration. Ph.D. Thesis, University of Grenoble: Francais, **2009**; p 221. This figure was dedicated to the Public domain (HAL Open Science) by the creator. https://theses.hal.science/tel-00495316.

3.3. Formation of the Curved Crystallization Front.

Let us now consider the conditions of the CF curvature, leading to the emergence of a complete thermodynamic equilibrium of phases on the TL. This is possible at small values of the equilibrium contact angle θ when nucleation on the TL is difficult.

As mentioned above in Section 3.2, for the NW growing with a finite rate and having a transverse singular face adjacent to the TL, the thermodynamic equilibrium at point A is incomplete since it is obvious that some overcooling (supersaturation) of $\Delta T/T_E$ is required for the growth of the flat face. So, from a thermodynamic point of view, the critical condition is expressed via the radius of curvature.

With a positive deviation of the temperature ΔT from T_E in the droplet of the catalyst, the maximum concentration

https://doi.org/10.1021/acsomega.2c06475
ACS Omega 2023, 8, 8263−8275

Table 1. Results of Calculation ξ_2 and r_c for the NW Growth in the AuAl−Si System

NW radius r (nm)	200		100		50		10	
$\Delta T/T_E$	0.02	0.04	0.02	0.04	0.02	0.04	0.02	0.04
curvature of the crystallization front $\xi_2 \times 10^{-7}$ (m^{-1})	18.79	37.21	19.20	37.58	19.90	38.31	25.00	44.16
radius of curvature of CF r_c (nm)	5.32	2.69	5.20	2.59	5.03	2.61	4.00	2.26

(solubility) of the crystallizable substance, corresponding to the equilibrium at temperature T_E, decreases. The thermodynamic G_p potential and chemical potential μ decrease in this case too. Then, according to Le Chatelier's principle, in the system, we will start to have processes going in the direction that prevents a decrease in solubility with a deviation of ΔT. Namely, during crystallization, a curvature toward the liquid phase of the solid/liquid interface leads to an increase in solubility (an increase in ΔG_p and μ), corresponding to the convex surface of the CF. Therefore, to change the thermodynamic potential ΔG_p on the NW CF, we have two opposite trends: (i) one is due to the deviation of the equilibrium temperature of the separation of the crystallizable substance from the nanoscale droplet of the catalyst ΔT from the equilibrium T_E, and consequently, due to the decrease in the equilibrium solubility of the crystallizable substance, and (ii) the other one is determined by an increase in the limited concentration (solubility) of this substance caused by an increase of the curvature of the interface (Kelvin effect) during crystallization.[17]

The equilibrium of the liquid and solid phases means the equality of their chemical potentials at the interface, i.e., $\tilde{\mu}_L = \tilde{\mu}_S$. Thus, the complete phase equilibrium on the TL can be achieved at some combination of temperature T and TL radius of curvature r_c when the free energy exactly compensates ΔT deviation from an equilibrium T_E. The free energy is due to the increased solubility over the convex region of the solid/liquid NW interface surface. Thus, in the catalyst droplets, a very important thermodynamic size effect of the overcooling (supersaturation) reduction of $\Delta T/T_E$ is manifested. The result of this effect is the distortion of the CF and, in fact, the crystallization process itself.

The curvature of the CF occurs as follows. At low values of the difference $(\theta - \varphi_0)$, the steps on the TL under the droplet cannot be absorbed by the TL due to the energy disadvantage of the process since, for example, for cylindrical NWs: $\alpha_S - \alpha_L \cos\varphi_0 > \alpha_{SL}$. In this case, the steps will accumulate in front of it, forming curved surfaces deviated from a singular orientation[19,24] (Figures 4 and 9b). The CF under the drop of the catalyst consists of a central transversal flat region, most often with the {111} orientation, and of nonsingular areas near the three-phase interface. Therefore, the central face of the front is separated from the TL by a curved peripheral section with an angle of inclination ψ at point A (Figure 9b). The peripheral areas of the CF deviated from the singular orientation will contain many steps and require significantly less overcooling (supersaturation) $\frac{\Delta T}{T_E}$ for their growth. With a sufficiently large curvature of the CF on the TL itself at point A, the supersaturation can turn to zero so that a complete thermodynamic equilibrium ($\tilde{\mu}_L = \tilde{\mu}_S$) occurs.

The curvature of CF at point A on the TL consists of azimuthal ξ_1 and meridional ξ_2 curvature: $\xi_1 + \xi_2$. Azimuthal curvature ($\xi_1 = 1/r$, where r is the NW radius) changes slightly on a small curved section of length comparable to the NW diameter (5−100 nm). At the same time, the radius r_c of meridional curvature $\xi_2 = 1/r_c$ varies over a section of the same length from a few/tens of nanometers to infinity (Figure 9). Therefore, in the equations describing the equilibrium of phases at the top of the NW, ξ_2 plays a major role.

Further, to derive the equilibrium condition near the TL, several assumptions must be made. Here, we assume that the SFSE of the interfaces is positive, and the angle β is obtuse, $\beta > 90°$ (Figure 9). We consider an isotropic model of interface surfaces. In addition, we imply that the radius of curvature of the CF r_c is quite large compared to the size of the atoms. We also assume that chemical compounds do not form in binary liquids.

Let $\Delta\bar{\mu}_{LS}$ still express the difference in the free energy of the liquid and solid phases per atom. Given the curvature of the catalyst droplet, we can assume that for NWs under equilibrium conditions, the magnitude of the chemical potential or excess solubility of a solid with a convex surface occurring on the curved CF under the drop is equal to the difference in atomic free energy that would exist between the solid and liquid phases at $T_E - \Delta T$. Then, the equation for the chemical potential of the curved solid phase can be written as

$$\tilde{\mu}_S = \bar{\mu}_L - q\frac{\Delta T}{T_E} + \alpha_{SL}\Omega_S\xi_2 + \frac{\alpha_S\Omega_S}{r} \tag{13}$$

Considering that the curvature of the liquid phase is given by eq 8, we can rewrite eq 13 as

$$\tilde{\mu}_L - \tilde{\mu}_S = q\frac{\Delta T}{T_E} + \frac{2\alpha_L\Omega_L}{R} - \alpha_{SL}\Omega_S\xi_2 - \frac{\alpha_S\Omega_S}{r} \tag{14}$$

As mentioned above, at equilibrium on a curved CF, we have $\tilde{\mu}_L = \tilde{\mu}_S$. From eq 14, we get the meridional curvature ξ_2

$$\xi_2 = \frac{1}{\alpha_{SL}\Omega_S}\left(q\frac{\Delta T}{T_E} + \frac{2\alpha_L\Omega_L}{R} - \frac{\alpha_S\Omega_S}{r}\right) \tag{15}$$

Since the radius of the catalytic drop is $R = r/\cos\varphi$ (see ref 2), from eq 15, we get

$$\xi_2 = \frac{1}{\alpha_{SL}\Omega_S}\left(q\frac{\Delta T}{T_E} + \frac{1}{r}(2\alpha_L\Omega_L\cos\varphi - \alpha_S\Omega_S)\right) \tag{16}$$

From eqs 15 and 16, it can be seen that the curvature of the stepped surface of CF ξ_2 is determined by the magnitude of the NW radius r, the angle φ_0, and overcooling $\Delta T/T_E$. Indeed, atoms should go from the convex surface of the crystal into the liquid phase more easily than from the flat phase because they, on average, have weaker bonds, as the number of the nearest neighbor atoms is smaller. This effect depends on the radius of curvature r_c. Therefore, the equilibrium for greater overcooling $\Delta T/T_E$ is achieved at a greater curvature ξ_2. Thus, as will be said later, the steps accumulate before the TL can be absorbed by it with an increase of overcooling (supersaturation) in the droplet.

Using eq 15, we will evaluate the equilibrium curvature of the CF ξ_2 and the radius of curvature r_c at the wetting perimeter of the droplet for system AuAl−Si. For the

https://doi.org/10.1021/acsomega.2c06475
ACS Omega 2023, 8, 8263−8275

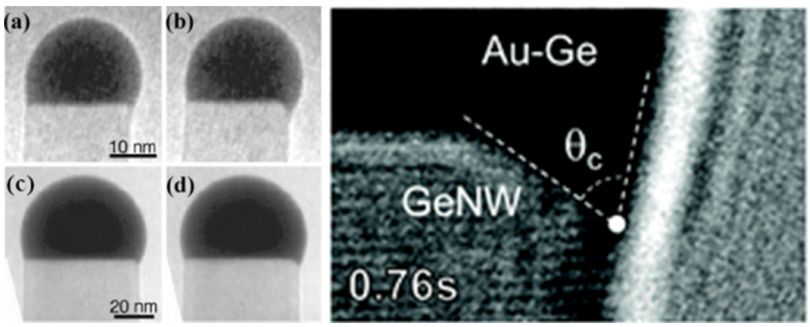

Figure 11. Left: frame-by-frame TEM images of the Si NW tops with a diameter of 23 nm, growing at T = 833 K and Si_2H_6 pressure $p = 1.07 \times 10^{-3}$ Pa with AuAl−Si particles (a, b) and Si NWs with a diameter of 60 nm, grown at T = 773 K and ~Si_2H_6 $p = 1.33 \times 10^{-3}$ Pa with AuGa−Si particles (c, d) illustrating the curvature of the crystallization front in the vicinity of the TL. Reprinted with permission from Wen, C.-Y.; Tersoff, J.; Hillerich, K.; Reuter, M.C.; Park, J. H. Periodically Changing Morphology of the Growth Interface in Si, Ge, and GaP Nanowires. Phys. Rev. Lett. **2011**, *107*, 025503. Copyright 2011 American Physical Society. Right: TEM image of Ge NW top showing the formation of a flat inclined face near the TL on a curved CF region in the Au−Ge system. Reprinted with permission from Gamalski, A. D.; Ducati, C.; Hofman, S. Cyclic Supersaturation and TPB Dynamics in Ge NW Growth. J. Phys. Chem. C **2011**, *115*, 4413−4417. Copyright 2011 American Chemical Society.

calculation, we use the following values: α_S = 1.230 J/m^2, α_L = 0.900 J/m^2, α_{SL} = 0.450 J/m^2, $\Omega_S = 2.0 \times 10^{-29}$ m^3, and φ = 30°.[17,19] In the calculations for Si, we use the specific heat of melting per atom $q = 8.3 \times 10^{-20}$ J.[23] Results of these calculations are presented in Table 1.

Table 1 shows that at given values of $\Delta T/T_E$ and φ with a decrease of the NW radius r, the curvature of the CF ξ_2 increases, and the radius of curvature r_c decreases. This fact is explained by an increase in the chemical potential or equilibrium solubility of the crystallizable substance at $r \to 0$. With an increase of $\Delta T/T_E$, the curvature of the front ξ_2 increases and the radius of curvature r_c decreases. If, for example, for Si, we take the thickness of the monoatomic layer h = 0.31 nm,[9] then ~17 atomic layers will be required to form the equilibrium curvature of the solid/liquid interface in the vicinity of the TL with r_c = 5.2 nm.

Let us now find an expression for angle ψ, which describes the curvature of the CF on the TL. An equilibrium on the TL is achieved if the sum of the force vectors corresponding to the SFSE of the interfaces (and their projections on the coordinate axis) is zero ($\varphi = \varphi_0$)

$$\begin{cases} -\alpha_S + \alpha_L \cos\varphi_0 + \alpha_{SL} \sin\psi = 0 \\ -\alpha_L \sin\varphi_0 + \alpha_{SL} \cos\psi = 0 \end{cases} \quad (17)$$

By solving the system of eq 17, we can express the angle of crystallization φ_0 as

$$\varphi_0 = \cos^{-1}\left(\frac{\alpha_S^2 + \alpha_L^2 - \alpha_{SL}^2}{2\alpha_S\alpha_L}\right) \quad (18)$$

Equation 18 shows that in the case of a CF distortion, the increment of the free energy of the three-phase system with the displacement of the TL in the direction of the continuation of the existing lateral surface of the NW is zero, and the formation of the NW surface under the angles other than φ_0 leads to an increase of free energy and is, therefore, impossible.[27] Hence, φ_0 is the angle of the equilibrium displacement of the TL. In the case when φ_0 = 90° and $\alpha_S > \alpha_{SL}$, a phase transition is possible only at the interface with a vapor.

The curvature of the crystallization front was also observed in refs 9 and 10 for NW grown in the AuAl−Si, AuGa−Si, and Ge−Au systems. The CF is curved in the case of good wettability of the crystal surface by a catalyst drop, as we can observe, for example, in the systems AuAl−Si, AuGa−Si, Au−Ge, Au−Si, etc. Figure 11 (left) shows the frame-by-frame TEM images of the Si NW tops obtained in ref 9, while Figure 11 (right) shows Ge NWs from ref 10.

At $\varphi = \varphi_0$, Si, Ge, GaAs, Si_xGe_{1-x}, and other NWs will grow with a constant diameter and vertical walls. At $\varphi < \varphi_0$, the crystal should expand, while at $\varphi > \varphi_0$, it should narrow down. Solving together the first equation from the system of eqs 17 and 18, we can express the angle ψ explicitly as

$$\psi = \sin^{-1}\left(\frac{\alpha_S^2 + \alpha_{SL}^2 - \alpha_L^2}{2\alpha_S\alpha_{SL}}\right) \quad (19)$$

It follows from eq 19 that the angle ψ of inclination of the curved section of the NW CF on the TL is also determined by the equilibrium conditions at the interface.

The values of angle φ_0 that make physical sense for the NW growth could be in the range of $0 < \varphi_0 < 90°$, see eq 18. This means that according to eq 17 at $\alpha_S > \alpha_L$ and positive values of the SFSE of the phase interfaces, angle $\psi > 0$. Hence, for a low-index facet AC exiting to the TL (see Figure 13 below) to appear at some point on the curved CF under the Me catalyst drop, we need the sections of the front near this point not to serve as a source of steps for the facet. To achieve this, it is necessary that the initial curved CF and the TL itself are convex: $\psi > 0$ and $r_c > 0$. The condition of TL convexity is necessary because, in certain cases, it may not be convex with respect to the crystal (for example, on the inner surface of a nanotube $r_c < 0$). If the facet is exiting to the TL, then the TL should change its rounded shape, and rectilinear areas will appear on it.

Experimental conditions for the formation of a convex crystallization front and the appearance of a chamfer (edge-truncation) on the edge of NW along the perimeter of wetting the catalyst droplet are implemented in refs 9−11 and 16 during the growth of GaAs, Al_2O_3, and other crystals. As we demonstrated above, the conditions of the formation of an inclined close-packed face (truncation) at the periphery of the CF depend on the magnitude of the contact angle β. The presence or absence of an oblique facet is responsible for the formation of the ZB or WZ structure of the GaAs NW.[8] Indeed, the polymorphic phase transition ZB ⇔ WZ occurs at two critical angles of $\beta \approx 100$ and 125°.[9] Therefore, by changing the volume of the catalyst drop by modulating the Ga

https://doi.org/10.1021/acsomega.2c06475
ACS Omega 2023, 8, 8263−8275

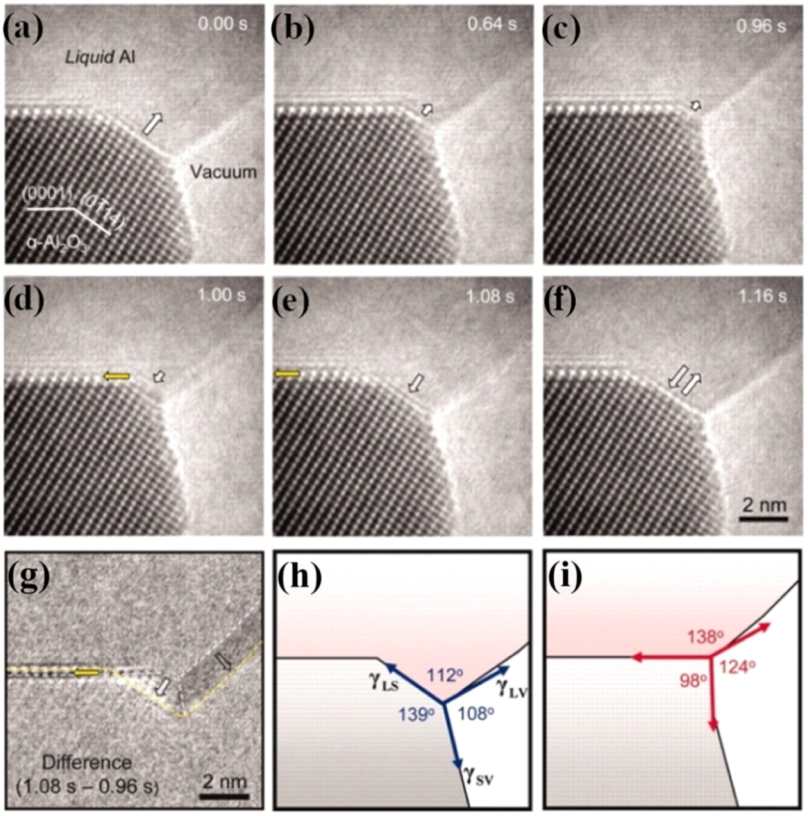

Figure 12. Frame-by-frame images of the change in the truncation area at the edge of the sapphire (α-Al_2O_3) NW, i.e., changes of the area of the singular inclined face adjacent to the TL. (a–f) Images were captured from a real-time movie[11] at the elapsed times shown. (g) The difference image obtained by subtracting the video image (c) from (e). (h, i) Schematic illustration of the triple-junction configuration during local crystal growth on the (0$\bar{1}$14) facet (h) and at the end of growth (i). Reprinted with permission from Oh, S. H.; Chisholm, M.F.; Kauffman, Y.; Kaplan, W. D.; Luo, W.; Ruhcle, M.; Scheu, C. Oscillatory Mass Transport in Vapor–Liquid–Solid Growth of Sapphire Nanowires. Science **2010**, *330* (6003), 489–493. Copyright 2010 The American Association for the Advancement of Science.

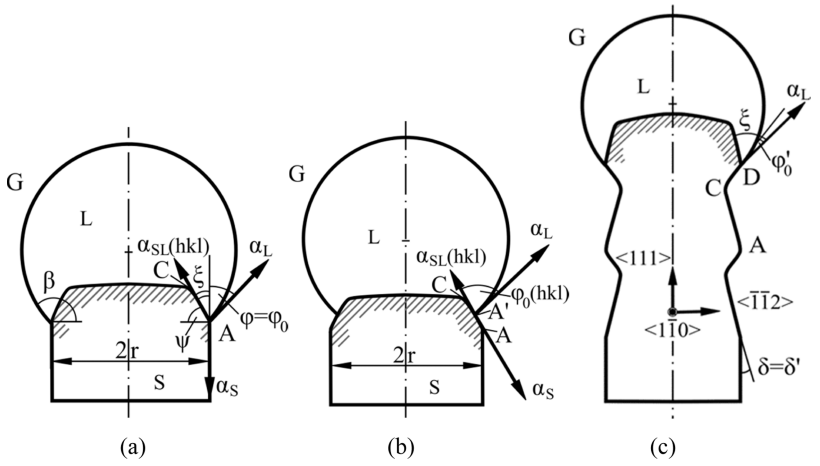

Figure 13. Scheme of different types of conjugation of the interfaces of three phases at the top of the NWs: (a) internal inclined close-packed facet AC adjacent to the TL appears on the CF; (b) the facet AC exits to the lateral surface of the NW; and (c) the formation of a sawtooth lateral surface ACD of the crystal.

or As stream, one can control the crystalline phase.[16] The control of the polymorphic modifications will allow one to avoid phase mixing and defects in the NW structure.[16]

Away from the TL, the curvature of the solid/liquid boundary decreases and tends to zero. Flat surfaces can form on the curved section of the front, which are truncated edges of the NW, adjacent to the TL and retaining energy-advantageous orientations {111}. During NW growth, these truncated edges can periodically change in area and, consequently, in the degree of truncation (Figure 12). The observed curved areas, as well as the complex geometry of the front with a truncated edge in the vicinity of the TL, are features of the certain growth conditions of Si, Ge, GaAs, GaP, α-Al_2O_3, and other NWs.[9−11] Moreover, according to important observations of Wen, Tersoff et al.,[9] and Gamalski et al.,[10] the degree of truncation depends on the level of supersaturation in the catalyst droplet.

https://doi.org/10.1021/acsomega.2c06475
ACS Omega 2023, 8, 8263−8275

It reaches its maximum when a new crystalline layer is added. For example, for Si NW, the thickness of the layer is 0.31 nm.[9] It has also been shown that the morphology of GaAs NW depends on the contact angle of the catalyst droplet.[16]

The exit of the inner face to the TL and the slippage of the drop along the inclined face can lead to the formation of a sawtooth outer surface of the NW, as shown in Figure 13c.[19]

At $\psi < 0$, the CF should be concave with a center of curvature in the liquid phase. If the curved part of the CF has a concave shape under the droplet (Figure 3a), then an additional supersaturation will occur above it due to the Gibbs−Thomson effect. Such supersaturation will lead to the degeneration of this part of the CF into a singular transverse face. By substituting the following values: $\alpha_L = 0.900$ J/m^2, $\alpha_S = 1.230$ J/m^2, and $\alpha_{SL} = 0.450$ J/m^2 for the AuAl−Si system into eqs 17 and 18, we get $\varphi_0 \approx 22.5°$ and $\psi \approx 45.9°$, respectively.

If, during the growth of the NWs, the CF or the TL are curved at a scale comparable to the size of the critical nucleus, it may change their volume, which is limited by the area of contact. This is demonstrated in Figure 14, where three nuclei with equal critical radii r^* and equal contact angles γ are shown.

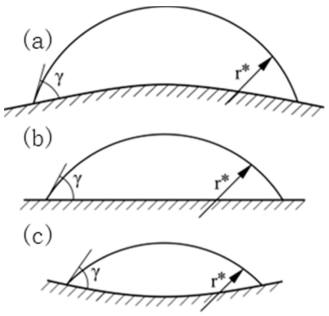

Figure 14. Formation of critical nuclei in the form of a spherical segment of the same radius of curvature r^* of the segmental surface and with the same contact angles γ on (a) the convex surface ($\psi > 0$), (b) the flat surface ($\psi = 0$), and (c) concave surface ($\psi < 0$) of the CF.

If the shape of the front or the TL is concave, then the volume of the spherical segment of the critical nucleus is clearly smaller so that its formation should occur with less overcooling. This fact is experimentally confirmed by the nucleus formation on either the "concavities" of the surface defects that have some "incoming" angles or on the "concave" TL at the NW growth.[19,28]

Let us define the relationship between the angles ψ and φ_0. To do this, we express from the second equation of the system of eq 16 the angle ψ

$$\psi = \arccos\left[\frac{\alpha_L}{\alpha_{SL}}\sqrt{1 - \cos\varphi_0^2}\right] \quad (20)$$

At $\psi = 0$, eq 20 becomes the classical expression $\varphi_0 = \sin^{-1}(\alpha_{SL}/\alpha_L)$,[26] when at $\alpha_L > \alpha_{SL}$, the flat transverse face of the CF is adjacent to the TL, while the curvature of the front is $\xi_2 = 0$. From eqs 17−19, we can conclude that if $\varphi_0 = \text{const}$, then the morphological stability of the CF described by the constant angle ψ will be observed during the NW growth.

3.4. Exit of the Internal Oblique Close-Packed Facet to the Lateral Surface of the Nanowire. At a sufficiently large curvature of the solid/liquid interface $r_c > 0$, an internal oblique close-packed facet AC (truncation[9−11,19]) may appear on the CF under the drop near the TL at an angle of $\psi > 0$ so that the new forming lateral surface of the NW will be inclined at an angle of $\xi = \beta - \varphi_0 - \psi$ to this facet (see Figures 11 (right), 12 and 13a). The formation of such an inclined (oblique) facet adjacent to the TL is possible due to the presence of singular minimums on the angular dependence of the SFSE. Therefore, under appropriate conditions, it is energetically beneficial for the inclined singular faces to appear on the lateral surface of a growing NW (e.g., faces {111} for Si and Ge with a diamond cubic structure or faces (111)B for GaAs with a zinc blende structure).

For the inclined close-packed facet {hkl} (Miller indices) of the CF adjacent to the TL to reach the lateral surface of the NW (Figure 13b,c), the difference between the free surface energy α_S (hkl) of the oblique facet and the sum of the projections of the force vectors corresponding to the surface energies α_L, α_{SL}, and α_S on this facet must be negative. In other words, the inequality $[\alpha_S(hkl) - (\alpha_S \cos\xi - \alpha_L \cos(\varphi + \xi) - \alpha_{SL}(hkl))] < 0$ must be held. In this case, the exit of the inclined facet {hkl} to the lateral surface of the NW will be energetically favorable. This difference becomes negative when $\alpha_S \cos\xi > \alpha_S(hkl)$ or $\xi < \cos^{-1}(\alpha_S(hkl)/\alpha_S)$.

Hence, starting from some critical angle $\xi^* = \cos^{-1}(\alpha_S(hkl)/\alpha_S)$ for all $\xi < \xi^*$ instead of the isotropic lateral surface of the NW at an angle $\xi = \beta - \varphi_0 - \psi$ to the face, an outer face is formed at a zero angle: $\xi = 0$. If initially $\varphi_0 + \xi < \theta(hkl)$, then the drop will slide along the inclined facet. It will reduce the wetting perimeter and increase the value of the already nonequilibrium angle φ_0 until the new equilibrium value of this angle $\varphi_0(hkl)$ at point A′ is set so that the sum of the projections of the three vectors corresponding to the free energies of the interfaces to the (hkl) facet is zero

$$\alpha_{SL}(hkl) = \alpha_S(hkl) - \alpha_L \cos\varphi_0(hkl) \quad (21)$$

In eq 21, the angle $\varphi_0(hkl)$ is equal to the angle of the wettability of the surface of the inclined facet by the melt of the Me catalyst $\theta(hkl)$: $\varphi_0(hkl) = \theta(hkl)$. Further movement of the drop along the inclined facet after point A′ (Figure 10b) will be difficult due to the free energy increase in this process. Thus, the inequality $\xi + \varphi_0 < \theta(hkl)$ is one of the conditions for the exit of the oblique close-packed facet (hkl) to the side surface of the NW.

However, for the oblique facet (hkl) to appear on the lateral surface of the NW, another initial condition $\xi > 0$ must be met; otherwise, the faceted portion of the TL is displaced by the neighboring regions similar to how the rapidly growing faces of a polyhedral crystal disappear. Thus, the criterion for the exit of an oblique close-packed facet (hkl) to the side surface of the NW can be expressed as the double inequality $0 < \xi < \theta(hkl) - \varphi_0(hkl)$, where $\xi < \cos^{-1}(\alpha_S(hkl)/\alpha_S)$. Figure 15 shows an SEM image of Si NW demonstrating the facetation of the side surface directly below the catalyst droplet.

In diamond-lattice crystals, the angles between the inner oblique facet of the {111} family and {111} transverse face can be ∼71.5 and ∼109.5° (±19.5° to the axis of the crystal).[30] The maximum area of the inclined facet will be observed during the greatest supersaturation in the drop when a new crystallization layer appears on the CF.[9] And the area of the oblique facet will decrease during the incubation period between the precipitation of the layers.

https://doi.org/10.1021/acsomega.2c06475
ACS Omega 2023, 8, 8263−8275

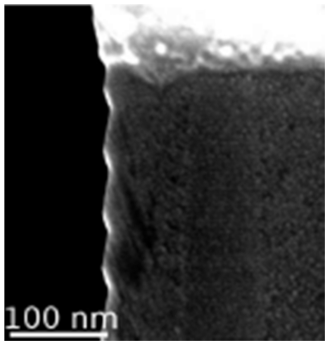

Figure 15. SEM image of Si NW, showing faceting of sidewall surface immediately below the catalyst droplet. Reprinted with from Dhalluin, F. Nanofils de Silicium: Dépôt chimique en phase vapeur assisté par catalyseurs métalliques et prémices d'intégration. Ph.D. Thesis, University of Grenoble: Francais, **2009**; p 221. This figure was dedicated to the Public domain (HAL Open Science) by the creator. https://theses.hal.science/tel-00495316.[29]

To estimate the value of ξ^* for Si, we take the initial value of the SFSE of $\alpha_S\{111\} \approx 1.230$ J/m^2.[17] Given that the ratios of the density of the broken bonds on the {211} and {110} faces representing the side surface of the NW to their densities on the {111} faces are 1.41 and 1.22,[23] respectively, we obtain $\alpha_S\{211\} \approx 1.734$ J/m^2 and $\alpha_S\{110\} \approx 1.500$ J/m^2. Therefore, the average SFSE of the side faces of the Si NW is $\alpha_S(\mathrm{Si}) \approx 1.617$ J/m^2. Then, we get $\xi^* = \cos^{-1}(1.230/1.617) \approx 40.5°$. Thus, at the angles $\psi = (90° - \xi^*) > 49.5°$, we should expect the exit of the oblique facet to the side surface of the Si NW, which corresponds to the {111} face at an angle of ~19.5° to the crystal axis (see Figure 5).

All of the results of this study fit into one scheme if we assume that the crystallization angle φ_0, the wetting angle θ, and the inclination angle ψ of the curved CF are determined from the condition of thermodynamic equilibrium. The spread of the experimental data should be explained by the deviation of the experimental conditions from equilibrium.[31,32] However, possible kinetic effects, e.g., the effect of anisotropy of free surface energy at the crystal/vapor interface, the effect of impurities on crystallization temperature, phase switching ZB ⇔ WZ, transverse temperature gradient etc., can affect the experimental results since in this case, the conjugation angle of the liquid and solid phases can be arbitrary.[33,34] However, all of the effects can be taken into account in the framework of the approach developed in this paper.

To summarize, we should note that the equilibrium between the solid and liquid phases separated by the curved surface of the NW CF with the critical radius r_c^* is unstable. Indeed, with even a slight temperature decrease, the rate of crystallization exceeds the rate of dissolution, which leads to NW growth. The decrease of the curvature of the CF under the drop due to crystallization increases the equilibrium temperature and accelerates the growth of the crystal. At a small temperature increase, the rate of dissolution of the crystal in the liquid phase of the catalyst exceeds the rate of crystallization, which results in part of the NW dissolution, and the radius of curvature of the CF decreases. The deviation from the equilibrium becomes greater, and the dissolution is accelerated; hence, the curvature of the CF disappears. These conclusions were confirmed by the experimental works by Wen, Tersoff et al.,[9] and Gamalski et al.,[10] etc., where the dependence of the level of truncation of the CF on the amount of supersaturation in the catalyst droplet was discovered. For example, in the photo Figure 11 (left), the level of the CF curvature of Si NW along the wetting perimeter of the Au−Si droplet is different. Therefore, for stable NW growth, a careful maintenance and precision control of supersaturation in the vapor phase, NW growth temperature, and the composition of the vapor phase are crucial.

Thus, in this paper, we developed a model based on the thermodynamic size effect of reduction of overcooling (oversaturation) in a drop of catalyst to explain the CF curvature under a drop in the process of NW growth. In this work, for the first time, the effect of reduction of overcooling on the resulting NWs is described. By controlling the size of the liquid phase, it is possible to significantly change the magnitude of the CF curvature and thus initiate or exclude the appearance of internal oblique facets by controlling the morphology and crystalline phase of the growing NWs.

4. CONCLUSIONS

In this paper, we analyzed the conditions leading to a change in the form of the NW CF and the causes of the formation of atomically smooth (singular) and curved (nonsingular) regions.

It is shown that under conditions of good wettability of the crystalline surface with a catalytic liquid and nucleation at regular places of the growing NW face at any temperature T below the equilibrium T_E, a thermodynamic size effect of the decrease of overcooling (supersaturation) in the Me catalyst droplets is manifested. The curvature of the CF is a result of this thermodynamic size effect. The free energy is due to the increased solubility of the substance crystallizable in the form of a NW over the convex region of the solid/liquid interphase surface.

It is shown that at a sufficiently large angle difference $(\theta - \varphi_0)$, under conditions when $\alpha_L > \alpha_{SL}$ and $\alpha_S > \alpha_L$, the CF coincides with the transverse singular face {111} adjacent to the TL at the top of a NW, the curvature of the front $\xi_2 = 0$ and the angle of equilibrium displacement of the TL $\varphi_0 = \beta - \delta$ is determined by eq 12.

With a small angle difference $(\theta - \varphi_0)$, and provided that $\alpha_L > \alpha_{SL}$, a metastable equilibrium is achieved on the CF near the TL due to the thermodynamic size effect of the reduction of overcooling (supersaturation), which results in the distortion of the CF.

The appearance of an inclined singular face on a curved section of the NW growth front is possible due to the dependence of the SFSE on the orientation of the face. It is shown that the criterion for the exit of an oblique, close-packed facet (hkl) to the NW side surface can be expressed via the double inequality $0 < \xi < \theta(hkl) - \varphi_0$, where $\xi < \cos^{-1}(\alpha_S(hkl)/\alpha_S)$.

These conclusions can only be applied to stationary NW growth.

AUTHOR INFORMATION

Corresponding Author

Elena V. Levchenko − *School of Information and Physical Sciences, College of Engineering, Science and Environment, University of Newcastle, Callaghan, NSW 2308, Australia;* orcid.org/0000-0003-3931-574X;
Email: elena.levchenko@newcastle.edu.au

https://doi.org/10.1021/acsomega.2c06475
ACS Omega 2023, 8, 8263−8275

Authors

Valery A. Nebol'sin − *Department of Radio Engineering and Electronics, Voronezh State Technical University, 394026 Voronezh, Russia*

Vladimir Yuryev − *Department of Radio Engineering and Electronics, Voronezh State Technical University, 394026 Voronezh, Russia*

Nada Swaikat − *Department of Radio Engineering and Electronics, Voronezh State Technical University, 394026 Voronezh, Russia*

Complete contact information is available at: https://pubs.acs.org/10.1021/acsomega.2c06475

Author Contributions

V.A.N. and N.S. performed the experiment. This manuscript was written through contributions of all authors. All authors have given approval to the final version of the manuscript.

Notes

The authors declare no competing financial interest.

■ ACKNOWLEDGMENTS

The study was carried out with the financial support of the Russian Foundation for Basic Research No. 22-22-00449 "Nanoelectronics and Nanotechnological Devices" https://rscf.ru/project/22-22-00449/ on the equipment of the Central Public Institution of Voronezh State Technical University.

■ REFERENCES

(1) Thelander, C.; Agarwal, P.; Brongersma, S.; Eymery, J.; Feiner, L.; Forchel, A.; Scheffler, M.; Riess, W.; Ohlsson, B.; Gösele, U.; Samuelson, L. Nanowire Base One-Dimensional Electronics. *Mater. Today* **2006**, *9*, 28−35.

(2) Ishikawa, F.; Buyanova, I. A. *Novel Compound Semiconductor Nanowires: Materials, Devices and Applications*; Pan Stanford Publishing: Singapore, 2018.

(3) Lieber, C. M. Semiconductor Nanowires: A Platform For Nanoscience And Nanotechnology. *MRS Bull.* **2011**, *36*, 1063.

(4) Natarajan, C. M.; Tanner, M. G.; Hadfield, R. H. Superconductor Science And Technology Superconducting Nanowire Single-photon Detectors: Physics And Applications Superconducting Nanowire Single-photon Detectors: Physics and Applications. *Supercond. Sci. Technol.* **2012**, *25*, No. 063001.

(5) Fang, X.; Bando, Y.; Gautam, U. K.; Ye, C.; Golberg, D. Inorganic Semiconductor Nanostructures And Their Field-emission Applications. *J. Mater. Chem.* **2008**, *18*, 509−522.

(6) Han, N.; Wang, F.; Yip, S. P.; Hou, J. J.; Xiu, F.; Shi, X.; Hui, A. T.; Hung, T. F.; Ho, J. C. GaAs nanowire Schottky barrier photovoltaics utilizing Au−Ga alloy catalytic tips. *Appl. Phys. Lett.* **2012**, *101*, No. 013105.

(7) Sun, J.; Han, M.; Gu, Y.; Yang, Z.-X.; Zeng, H. Recent Advances in Group III-V Nanowire Infrared Detectors. *Adv. Opt. Mater.* **2018**, *6*, No. 1800256.

(8) Harmand, J.-C.; Patriarche, G.; Glas, F.; Panciera, F.; Florea, I.; Maurice, J.-L.; Travers, L.; Ollivier, Y. Atomic Step Flow on a Nanofacet. *Phys. Rev. Lett.* **2018**, *121*, No. 166101.

(9) Wen, C.-Y.; Tersoff, J.; Hillerich, K.; Reuter, M. C.; Park, J. H.; et al. Periodically Changing Morphology of the Growth Interface in Si, Ge, and GaP Nanowires. *Phys. Rev. Lett.* **2011**, *107*, No. 025503.

(10) Gamalski, A. D.; Ducati, C.; Hofman, S. Cyclic Supersaturation and TPB Dynamics in Ge NW Growth. *J. Phys. Chem. C* **2011**, *115*, 4413−4417.

(11) Oh, S. H.; Chisholm, M. F.; Kauffman, Y.; Kaplan, W. D.; Luo, W.; Ruhcle, M.; Scheu, C. Oscillatory mass transport in vapour-liquid-solid growth of sapphire nanowires. *Science* **2010**, *330*, 489−493.

(12) Wang, F.; Wang, C.; Wang, Y.; Zhang, M.; Han, Z.; Yip, S. P.; Shen, L.; Han, N.; Pun, E. Y. B.; Ho, J. C. Diameter Dependence of Planar Defects in InP Nanowires. *Sci. Rep.* **2016**, *6*, No. 32910.

(13) Han, N.; Wang, Y.; Yang, Z.; Yip, S. P.; Wang, Z.; Li, D.; Hung, T. F.; Wang, F.; Chenab, Y.; Ho, J. C. Controllable III−V nanowire growth via catalyst epitaxy. *J. Mater. Chem. C* **2017**, *5*, 4393−4399.

(14) Jacobsson, D.; Panciera, F.; Tersoff, J.; Reuter, M. C.; Lehmann, S.; Hofmann, S.; Dick, K. A.; Ross, F. M. Interface dynamics and crystal phase switching in GaAs nanowires. *Nature* **2016**, *531*, 317−322.

(15) Dubrovskii, V. G. *Nucleation Theory and Growth of Nanostructures*; Springer-Verlag: Berlin, Germany, 2014; p 601.

(16) Panciera, F.; Baraissov, Z.; Patriarche, G.; Dubrovskii, V. G.; Glas, F.; Travers, L.; Mirsaidov, U.; Harmand, J.-C. Phase selection in self-catalysed GaAs nanowires. *Nano Lett.* **2020**, *20*, 1669−1675.

(17) Givargizov, E. I. Fundamental aspects of VLS growth. *J. Cryst. Growth* **1975**, *31*, 20−30.

(18) Gridchin, V. O.; Kotlyar, K.; Reznik, R.; Dvoretskaya, L. N.; Parfen'eva, A. V.; Mukhin, I. S.; Cirlin, G. E. Selective-Area Growth of GaN Nanowires on Patterned SiO_x/Si Substrates by Molecular Beam Epitaxy. *Tech. Phys. Lett.* **2020**, *46*, 1080−1083.

(19) Nebol'sin, V. A.; Shchetinin, A. A.; Korneeva, A. N.; Dunaev, A. I.; Dolgachev, A. A.; Sushko, T. I.; Tatarenkov, A. F. Development of Lateral Faces during Vapor−Liquid−Solid Growth of Silicon Whiskers. *Inorg. Mater.* **2006**, *42*, 339−345.

(20) Alekseev, P. A.; Sharov, V.; Borodin, B. R.; Dunaevskiy, M. S.; Reznik, R. R.; Cirlin, G. E. Effect of the Uniaxial Compression on the GaAs Nanowire Solar Cell. *Micromachines* **2020**, *11*, 581−593.

(21) Ek, M.; Filler, M. A. Atomic-Scale Choreography of Vapor−Liquid−Solid Nanowire Growth. *Acc. Chem. Res.* **2018**, *51*, 118−126.

(22) Wagner, R. S.; Ellis, W. C. Vapor-Liquid-Solid Mechanism of Single Crystal Growth. *Appl. Phys. Lett.* **1964**, *4*, 89−95.

(23) Nebol'sin, V. A.; Swaikat, N.; Korneeva, V. V. Mechanisms of Atomic−Molecular Processes Underlying Si and GaAs Nanowire Crystallization. *Inorg. Mater.* **2021**, *57*, 219−226.

(24) Nebol'sin, V. A.; Swaikat, N.; Vorob'ev, A. Y. Development of Growth Theory for VLS Nanowires: Wetting Scenario. Front Curvature. Growth Angle. Linear Tension. and Radial Instability. *J. Nanotechnol.* **2020**, No. 5251823.

(25) Glas, F.; Harmand, J. C.; Patriarche, G. Why does wurtzite form in nanowires of III-V ZB semiconductors? *Phys. Rev. Lett.* **2007**, No. 146101.

(26) Burton, W. K.; Cabrera, N.; Frank, F. C. The growth of crystals and the equilibrium of their surfaces. *Philos. Trans. R. Soc., A* **1951**, *243*, 299−358.

(27) McIntyre, P. C.; Fontcuberta i Morral, A. Semiconductor nanowires: to grow or not to grow? *Mater. Today Nano* **2020**, *9*, No. 100058.

(28) Nebol'sin, V. A.; Dunaev, A. I.; Vorob'ev, A. Y.; Samofalova, A. S.; Zenin, V. V. Formation of "Negative" Silicon Whiskers. *Inorg. Mater.* **2017**, *53*, 775−780.

(29) Dhalluin, F. Nanofils de Silicium: Dépôt chimique en phase vapeur assisté par catalyseurs métalliques et prémices d'intégration. Ph.D. Thesis, University of Grenoble: Francais, 2009; p 221. https://theses.hal.science/tel-00495316.

(30) Maliakkal, C. B.; Jacobsson, D. M.; Tornberg, M.; Persson, A. R.; Johansson, J.; Wallenberg, R.; Dick, K. A. In situ analysis of catalyst composition during gold catalyzed GaAs nanowire growth. *Nat. Commun.* **2019**, *10*, No. 4577.

(31) Schwarz, K. W.; Tersoff, J.; Kodambaka, S.; Chou, Y.-C.; Ross, F. M. Geometrical Frustration in Nanowire Growth. *Phys. Rev. Lett.* **2011**, *107*, No. 265502.

(32) Ross, F. M. Nanowires: Bringing order to twin-plane defects. *Nat. Nanotechnol.* **2009**, *4*, 17−18.

(33) Ghisalberti, L.; Potts, H.; Friedl, M.; Zamani, M.; Güniat, L.; Tütüncüoglu, G.; Carter, W. C.; Fontcuberta i Morral, A. Questioning liquid droplet stability on nanowire tips: from theory to experiment. *Nanotechnology* **2019**, *30*, No. 285604.

(34) Güniat, L.; Caroff, P.; Fontcuberta i Morral, A. Vapor Phase Growth of Semiconductor Nanowires: Key Developments and Open Questions. *Chem. Rev.* **2019**, *119*, 8958−8971.

https://doi.org/10.1021/acsomega.2c06475
ACS Omega 2023, 8, 8263−8275